


DFT and QTAIM Studies of the Spectrophotometrically Investigated V(V)-6-Chloro-3-hydroxy-7-methyl-2-(2'-furyl)-4H-chromen-4-one Complex

Nivedita Agnihotri ^{1,*} , Sonia Nain ², Navneet Kaur ³, Chetna Dhonchak ¹, Masrat Mohmad ¹, Rakesh Kumar ⁴, Sadegh Kaviani ⁵

¹ Department of Chemistry, Maharishi Markandeshwar (Deemed to be University), Mullana, Ambala – 133207, India

² Department of Chemistry, DCRUST, Murthal, Sonapat-131039, India

³ Emax International School, Ambala, India

⁴ Department of Chemistry, MCM DAV College, Kangra (HP)-176001, India

⁵ Institute of Physics, Kazan Federal University, 420008 Kazan, Russia

* Correspondence: nivagnil1@gmail.com (N.A.);

Received: 6.11.2023; Accepted: 7.01.2025; Published: 30.12.2025

Abstract: A simple and rapid solvent extraction technique was used to study the extractive formation of a binary complex between vanadium (V) and 6-chloro-3-hydroxy-7-methyl-2-(2'-furyl)-4H-chromen-4-one (CHMFC). In a mildly acidic medium containing 0.9-1.5 ml of 0.2% ethanolic solution of the ligand, CHMFC interacts with vanadium in its pentavalent state to generate a yellow complex. With a correlation coefficient of 0.9987, the 1:2 (M:L) color system obeys linearity from 0.199-0.865 ppm of vanadium in the organic solution of dichloromethane. At 425 nm, molar absorptivity, Sandell's sensitivity, and standard deviation are $6.011 \times 10^4 \text{ l mol}^{-1} \text{ cm}^{-1}$, 0.00085 $\mu\text{g V(V) cm}^{-2}$ and ± 0.0018 , respectively. The suggested approach is satisfactorily applied to numerous samples of analytical interest. To explore the basic structure, bonding features, and stability, the thus-produced V(V)-CHMFC complex was subjected to DFT calculations. Finally, to characterize the nature and type of various interactions in the presented complex system, QTAIM analysis was used successfully.

Keywords: Vanadium; 6-Chloro-3-hydroxy-7-methyl-2-(2'-furyl)-4H-chromen-4-one; Extraction; Spectrophotometric determination; DFT; QTAIM; Analytical; Theoretical Studies.

© 2025 by the authors. This article is an open-access article distributed under the terms and conditions of the Creative Commons Attribution (CC BY) license (<https://creativecommons.org/licenses/by/4.0/>), which permits unrestricted use, distribution, and reproduction in any medium, provided the original work is properly cited. The authors retain copyright of their work, and no permission is required from the authors or the publisher to reuse or distribute this article, as long as proper attribution is given to the original source.

1. Introduction

Vanadium, a hard, silvery-grey, malleable transition metal that resists corrosion, was obtained in 1867 by Henry Roscoe in its pure form [1]. The symbol V is based on the fantoccini of the Scandinavian Goddess of beauty, Vanadis. The name vanadium was assigned because of the wide range of colors of its compounds [2]. Vanadium is found in about 65 minerals, including vanadinite, carnotite, and patronite. It is also found in phosphate rocks, certain iron ores, and some crude oils in the form of organic complexes. The pure metal is soft, has good structural strength, and exhibits excellent corrosion resistance to alkalies, mineral acids, and saline water.

The most important use of the metal is as a steel additive. Vanadium steel alloys are very tough and are used for axles, tools, piston rods, armor plates, and antilock braking systems (ABS). Vanadium alloys find their utility in nuclear applications. Vanadium foil is also used to bond titanium to steel. The other important applications of vanadium compounds include

acting as a catalyst in the manufacture of aniline black and as a mordant in the printing and dyeing of fabrics [3]. Biologically, vanadium is essential to some species, including human beings [4-6]. However, in some compounds, vanadium is toxic and requires care while handling. The health benefits of vanadium involve using vanadium supplements as medicine. The metal is also used to treat diabetes, low blood sugar, high cholesterol, heart problems, TB, syphilis, and edema, and to prevent cancer [4-6].

Thus, the significant commercial and biological use of vanadium underscores the need to develop methods for its determination; the approach is authentic, rapid, sensitive, and selective. For this reason, UV-VIS spectrophotometry [7-14] is found to be the most fruitful due to its severity, reasonable cost, and capability to produce sensitive, selective, highly accurate, precise, and reproducible results over a number of other techniques [15-22] that can be employed for analytical purposes.

The presented analysis accounts for the simple, fast, sensitive, selective, and direct spectrophotometric technique for the determination of trace amounts of vanadium in its pentavalent oxidation state. The target is achieved by the formation of a complex between vanadium (V) and the color-forming reagent, 6-chloro-3-hydroxy-7-methyl-2-(2'-furyl)-4*H*-chromen-4-one (CHMFC), which offers the advantage of high stability, rapidity, reproducibility, sensitivity, and selectivity over a number of previously reported similar methods [7-14]. The hence studied spectrophotometric analysis is subjected to the DFT calculations and QTAIM analysis for a better understanding of V(V)-CHMFC complex, for evaluating molecular structure, stability, reactivity, the values of electron density and its Laplacian as well as total energy density, kinetic energy density and potential energy density of the interatomic contacts between the ligand and metal cation for the complex.

2. Materials and Methods

2.1. Equipment, reagents, and solutions.

For optical density measurements and spectroscopic studies, an Electronics India double-beam 2375 UV-Visible spectrophotometer with 10 mm path-length quartz cells was employed.

All materials and reagents used in the analysis were of analytical quality. A 1 mg ml⁻¹ vanadium (V) stock solution was prepared by dissolving 239 mg of sodium metavanadate (NaVO₃; CDH) in 100 ml of doubly deionized water and volumetrically standardized using the ferrous sulfate method [23]. Working solutions of 10 and 5 µg ml⁻¹ were obtained by appropriately diluting aliquots.

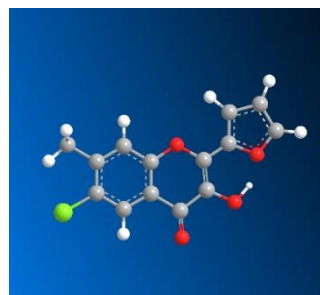
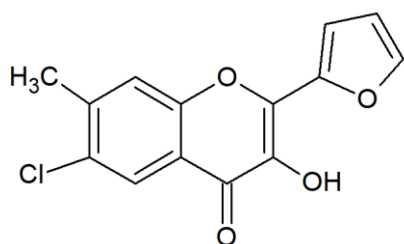


Figure 1. CHMFC.

6-Chloro-3-hydroxy-7-methyl-2-(2'-furyl)-4*H*-chromen-4-one (CHMFC); Molecular formula = C₁₄H₉O₄Cl; molar mass = 276.5 g mol⁻¹ was synthesized by the AFO reaction as reported [24] and 0.1% or 0.2% [(w/v); as per requirements] solutions were set up by dissolving

the suitably measured samples in ethanol. The structure of the complexing agent is shown in Figure 1.

By suitable dilution of the icy glacial acid, its 2M solution was prepared to be used for analysis. Dichloromethane (CDH) was used as such for extraction.

The synthetic mixtures, some equivalent to nichroloy, palau, permendur, and crocar were prepared as per Table 1 for analysis. The industrial steel samples and reverberatory flue dust were brought into solution as described earlier [14], adjusted to 0.24 M acetic acid, and the metal ions were determined according to the suggested procedure (Table 1).

2.2. Computational methods.

DFT calculations were performed using the Gaussian 09 (Revision B.04) package [25] to yield minimum-energy geometries, molecular orbitals (HOMO–LUMO), and other molecular characteristics. The geometry optimization was performed in the gaseous state. The optimized molecular structures, including HOMO and LUMO surfaces, were viewed using the GaussView 05 program [26]. The Vosko, Wilk, and Nusair 1980 local correlation functional (III) (B3LYP) [27] was used in conjunction with Becke's three-parameter hybrid-exchange functional and the Lee, Yang, and Parr nonlocal correlation expression. For C and O, the 6-31G(d,p) basis set was employed. During the theoretical work, the LANL2DZ basis set [28] and the Hay and Wadt pseudopotentials [29,30] were used. QTAIM analysis was performed for the studied complex at M06-2X/6-311++G(d,p) level.

Table 1. Analysis of various synthetic and technical samples.

S No.	Sample Composition		V(V) found ($\mu\text{g}/10\text{ml}$)**
	Matrix*	V(V) added ($\mu\text{g}/10\text{ml}$)	
1	Fe ^{III} (0.25), Ni(0.12), Cr(0.1), Mn(0.005) ^{a,b}	5	5.00
2	Ni(0.021), Pt(0.003), Pd(0.007) ^a	4	3.94
3	Fe ^{III} (0.25), Co(0.25), Mn(0.002) ^{a,b}	5	4.91
4	Fe ^{III} (0.37), Cr(0.06), Co(0.004) ^{a,b}	4	4.11
5	Mg(8), Mn(5), Mo ^c (0.02)	5	4.92
6	Pt(0.5), Pd(0.5), Ir(0.05)	8	8.05
7	Pb(5), W(0.1), Ba(3)	4	4.07
8	Os(0.05), Ir(0.01), Rh(0.05)	7	6.95
9	Pb(5), Zr ^b (0.1), Ca(3)	10	10.04
10	Reverberatory flue dust(100)	5	5.08
11	High-speed steel super rapid extra 500 (50) ^b	1% ^d	0.980%
12	BCS 241/1 High-speed steel ^b	1.57% ^d	1.56%
13	BCS 220/1 High-speed steel ^{b,c}	2.09% ^d	2.11%

*Number in parentheses indicates the amount of metal ion in mg/10 ml. **Average of triplicate analysis;

^aComposition analogous to nichroloy, palau, permendur, and crocar, respectively. ^bIn presence of 5 mg sodium fluoride; ^cIn presence of 50 mg sodium phosphate.

2.3. Recommended procedure for the extraction spectrophotometric determination.

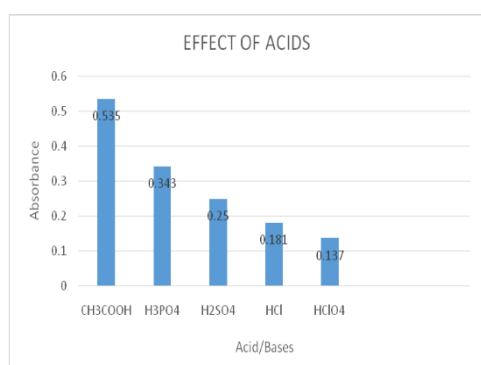
An aliquot of the sample form containing up to 11 μg vanadium (V) was mixed at room temperature with 1.0 ml of 2 M acetic acid, 1.2 ml of 0.2 percent ethanolic CHMFC solution, and enough deionized water to make a final aqueous volume of 10 ml. It was then equilibrated for 30 seconds with an equal volume (10 ml) of dichloromethane. After clear phase separation, the yellow organic phase was passed through a Whatman filter paper (No. 41, pretreated with the solvent) to remove any water droplets, and the yellow extract's absorbance was measured

at 425 nm against a reagent blank prepared in the same way. The amount of vanadium (V) was then calculated using the proposed approach and the calibration curve.

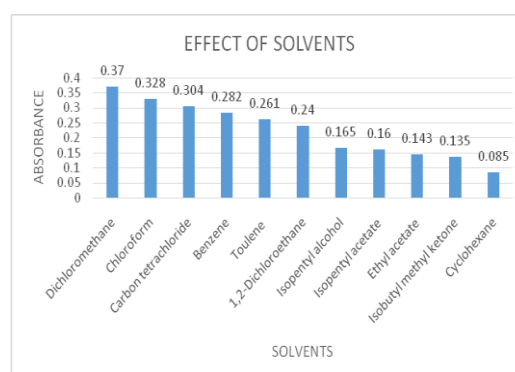
The procedure, however, was amended for samples containing Fe(III), Zr(IV), and Mo(VI). Where 5 mg of sodium fluoride was added as a masking agent each for 0.5 mg Fe (III) and 0.2 mg Zr (IV), 50 mg sodium phosphate was used to mask interference caused by up to 0.05 mg Mo (VI). The masking agents were mixed with the reaction mixture before adding the reagent.

3. Results and Discussion

An extractable yellow complex is formed between vanadium (V) and CHMFC at room temperature in a weakly acetic acid medium. In the strong acids like H₃PO₄, H₂SO₄, HCl, and HClO₄, colour is not stable, and also the colour intensity is observed to decrease in the same order as is shown in Bar Chart 1. The developed V(V)-CHMFC complex could be smoothly extracted into a number of non-aqueous organic solvents, as presented in Bar Chart 2. Dichloromethane, which provides the complex with maximum and sufficiently stable absorbance (for more than 2 days), is selected as the most appropriate extractant for further studies.



Bar Chart 1. Absorbance variation of V(V)-CHMFC complex with acids.



Bar Chart 2. Absorbance variation of V(V)-CHMFC complex with solvents.

Table 2. Effect of physical parameters on the absorbance of V(V)-CHMFC complex.

CH₃COOH^a/M	0.02	0.04	0.08	0.12	0.16-0.40	0.42	0.44	0.50
Absorbance	0.150	0.240	0.336	0.350	0.370	0.345	0.330	0.280
CHMFC^b/ml	0.1	0.3	0.5	0.6	0.8	0.9-1.5	1.6	1.8
Absorbance	0.050	0.190	0.270	0.330	0.470	0.590	0.548	0.490
Equilibration time^c/ s	0	2	5	10-180				
Absorbance	0.050	0.188	0.565	0.590				

Conditions :^aV(V) = 10 µg ; CH₃COOH(M) = Variable ; CHMFC [0.1% (w/v) in ethanol]=0.5 ml ; aqueous volume = solvent volume = 10 ml; solvent = dichloromethane; equilibration time = 30 s ; λ_{max} = 425 nm. ^bV(V) = 5 µg ; CH₃COOH = 0.2 M; other conditions being the same as in (a) except for variation in CHMFC concentration. ^c V(V) = 5 µg ; CHMFC [0.2% (w/v) in ethanol] = 1.2 ml ; other conditions being the same as in (b) excepting variation in equilibration time [CHMFC = 6-Chloro-3-hydroxy-7-methyl-2-(2'-furyl)-4H-chromen-4-one (CHMFC)].

The influence of various physical variables, including acidic strength, CHMFC concentration, and equilibration time, on the extraction determination of V(V) has been studied. It was analyzed that to attain the optimum and constant intensity of complex containing ≤ 11 µg V(V) in 10 ml aqueous phase, 0.16-0.40 M CH₃COOH and 0.9-1.5 ml of 0.1% (w/v) ethanolic solution of CHMFC added in the same order as per the applied procedure are

adequate (Table 2). The aqueous mixture thus obtained was equilibrated once with an equal volume of dichloromethane for 10-180 s.

3.1. Interference studies.

To investigate the selectivity and tolerance limit of the V(V)-CHMFC complex, the effect of various anions/complexing agents and cations was investigated by adding them (before the reagent) under identical conditions to the recommended policy, as shown in Tables 3 and 4. Among the several foreign ions investigated, hydrogen peroxide, ascorbic acid, oxalate, and ‘Disodium’ EDTA interfered significantly, even in tiny amounts.

Table 3. Effect of anions/complexing agents on V(V)-CHMFC complex.

S.No.	Anion/Complexing Agent Added	Tolerance limit	Absorbance
S.No.	Anion/complexing agent		
1	None	-	0.590
2	Sodium chloride, Sodium bromide, Sodium sulfate, Sodium nitrite, Sodium carbonate, Sodium sulfite, Thiourea, Sulfosalicylic acid, Hydrazine sulfate,	100	0.590
3	Potassium thiocyanate, Potassium iodide, Sodium phosphate	50	0.590
4	Sodium Nitrate	20	0.590
5	Potassium fluoride, Sodium potassium tartrate, Sodium acetate	5	0.590
6	Sodium Citrate	1	0.590
7	Glycerol	0.5*	0.590
8	‘Disodium’ EDTA**	0.5	0.035
9	Sodium oxalate**, Ascorbic acid**	0.1	0.160, 0.133
10	Hydrogen peroxide (6 % w/v)**	0.1*	0.062

*Amount added in ml; **Seriously interfere.

3.2. Spectral characteristics, Beer’s law, sensitivity, and statistical data.

The absorption spectrum of V(V) – CHMFC complex in DCM against reagent blank at the ideal state conditions shows an absorption maximum (λ_{max}) falling in the range 420 - 435 nm (Figure 2; curve a). The spectrum of the reagent blank against pure solvent shows that the reagent also absorbs a little at the working wavelength range (Figure 2; curve b). The best-fit curve for the complex justifies the validity of Beer’s law in the vanadium concentration range of 0.0 – 1.1 $\mu\text{g ml}^{-1}$ (Figure 3). However, the optimum range for accurate determination of vanadium as obtained from the Ringbom plot [31] at 425 nm is 0.199-0.865 $\mu\text{g V(V) ml}^{-1}$ (Figure 4). The calculated values of molar absorptivity, Sandell’s sensitivity, and the various statistical parameters have been compiled in Table 5.

Table 4. Effect of cations on V(V)-CHMFC complex.

S.No.	Cation Added*	Tolerance limit (mg/10 ml)	Absorbance
1	None	-	0.590
2	Al(III), Pb(II), Hg(II), Ba(II), Co(II), Mg(II), Mn(II), Zn(II), Ni(II), Sr(II)	10	0.590
3	Cd(II), Be(II), Ca(II), Cd(II)	8	0.590
4	La(III), Cu(II), Ag(I)	5	0.590
5	Se(IV), Pt(IV), Ti(IV), Cr(III), As(III), Bi(III), Sr(II), Pd(II)	1	0.590
6	Ce(IV), Cr(VI), Nb(V), Au(III), Fe(III) ^a	0.5	0.590
7	W(VI), Zr(IV) ^a , Fe(II)	0.2	0.590
8	Ir(III), Rh(III), Os(VIII)	0.1	0.590
9	Mo(VI) ^b , Sn(II)	0.05	0.590

*Initial oxidation state is shown in parentheses. ^aIn presence of 5 mg sodium fluoride; ^bIn presence of 50 mg sodium phosphate.

3.3. Stoichiometry of V(V)-CHMFC complex.

Job's continuous variations approach[32], adapted for a two-phase system by Vosburgh and Cooper[33] (Figure 5), and the mole ratio method[34] (Figure 6) have all established and validated the 1:2 (M:L) stoichiometric ratio of the V(V)-CHMFC complex.

Table 5. Optical characteristics and statistical parameters.

S. No.	Parameter	Value
1.	λ_{\max} (nm)	420 – 435
2.	Beer's law limit ($\mu\text{g ml}^{-1}$)	0 – 1.1
3.	Ringbom range (ppm)	0.199-0.865
4.	Molar absorptivity ($\text{l mol}^{-1} \text{cm}^{-1}$)	6.011×10^4
5.	Sandell's sensitivity ($\mu\text{g cm}^{-2}$)	0.00085
6.	Correlation coefficient (r)	0.9987
7.	Regression equation (Y) *	$Y=1.183 X + 0.0042$
8.	Slope (b)	1.183
9.	Intercept (a)	0.0042
10.	Standard deviation	0.0018
11.	Relative standard deviation (%)	0.298
12.	Limit of detection ($\mu\text{g ml}^{-1}$)	0.0559

* $Y = bX + a$; where Y = absorbance and X = Concentration of V(V) in $\mu\text{g ml}^{-1}$

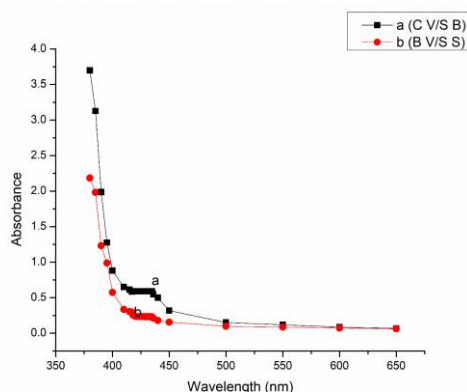


Figure 2. Absorption spectra of V(V)- HMFC complex: **a** – Complex against reagent blank; **b** – Reagent blank against pure DCM $0.5 \mu\text{g V ml}^{-1}$, other conditions as cited in the procedure.

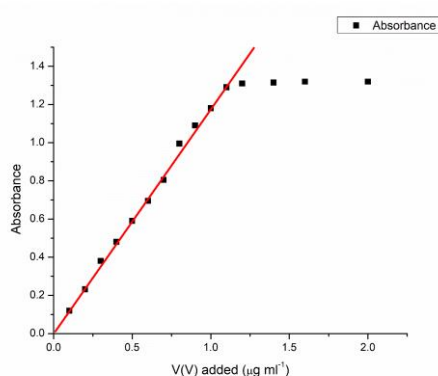


Figure 3. Beer's law range of V(V)-CHMFC complex.

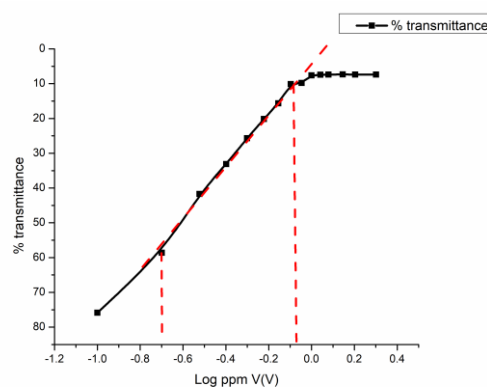


Figure 4. Ringbom plot for V(V)-CHMFC complex.

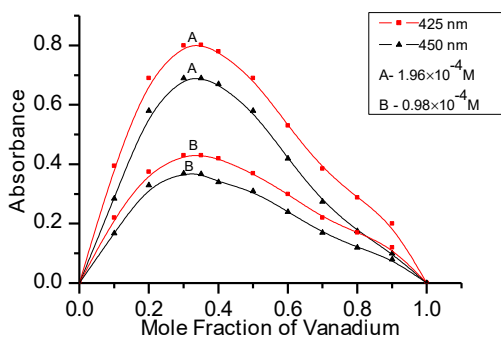


Figure 5. Job's continuous variations method.

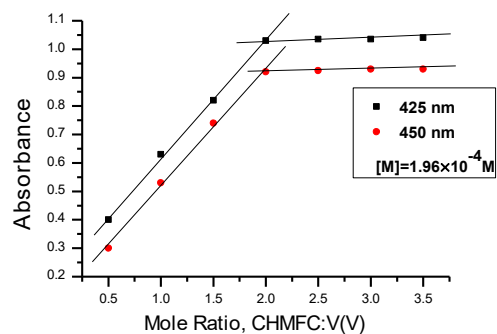


Figure 6. Mole ratio method.

The results obtained above are indicative of the following proposed structure, along with the optimized structure of the V(V)-CHMFC complex (Figure 7).

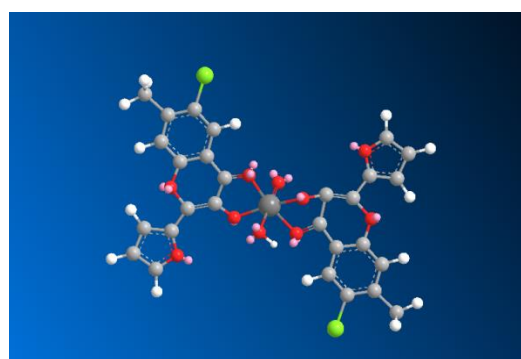
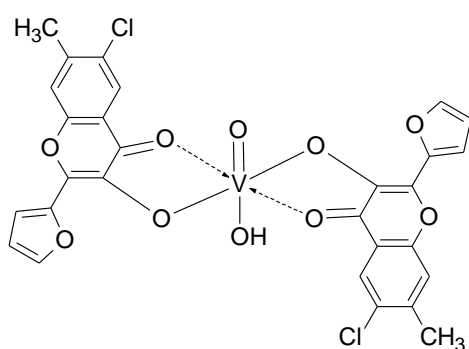


Figure 7. V(V)-CHMFC Complex.

Various properties of the optimized structure are given in Table 6.

Table 6. Bond parameters of the optimized structure of V(V)-CHMFC complex.

S No.	Bond Length		Bond angle	
	Atom type	Bond length (Å)	Atom type	Bond angle (°)
1	V(39)-O(41)	1.8714	O(41)-V(39)-O(37)	73.7706
2	O(37)-V(39)	1.8909	O(37)-V(39)-O(38)	63.3635
3	O(18)-V(39)	1.8889	O(18)-V(39)-O(40)	80.9475
4	O(38)-V(39)	1.8736	O(38)-V(39)-O(40)	86.9059
5	O(19)-V(39)	1.8792	O(18)-V(39)-O(19)	80.2804
6	V(39)-O(40)	1.6136	O(41)-V(39)-O(19)	72.3332

Table 7. Calculated HOMO-LUMO energy gap (E_g) and quantum molecular descriptors in eV.

Compound	E_{HOMO}	E_{LUMO}	E_g	I	A	η	S	M	Ω	ω^-	ω^+
CHMFC	-7.24	-1.26	5.98	7.24	1.26	2.99	0.33	-8.50	12.08	5.51	1.26
V(V)-CHMFC Complex	-7.03	-1.86	5.17	7.03	1.86	2.58	0.38	-8.89	15.31	6.37	1.92

3.4. Electronic properties.

The electronic properties such as HOMO-LUMO energy gap (E_g), ionization potential ($I = -E_{HOMO}$), electron affinity ($A = -E_{LUMO}$), electronic chemical hardness [$\eta = (I-A)/2$], chemical softness ($S = 1/\eta$), chemical potential [$\mu = -(I+A)/2$], electrophilicity index ($\omega = \mu^2/2\eta$), electron-donating power [$\omega^- = (3I+A)^2/16(I-A)$] and electron accepting power [$\omega^+ = (I+3A)^2/16(I-A)$] are investigated. The corresponding values are given in Table 7. The energy of HOMO (E_{HOMO}) is correlated with the ionization potential, whereas the energy of LUMO

(E_{LUMO}) corresponds to the electron affinity [35]. In the case of the ligand, the HOMO and LUMO levels are localized on the whole molecule at -7.24 eV and -1.26 eV, respectively, as shown in Fig. 8. After interaction of the ligand with vanadium metal cation, E_{HOMO} is increased from -7.24 eV to -7.03 eV and are located mostly on one of the ligand molecules, while the E_{LUMO} is shifted towards the lower energy value from -1.26 eV to -1.86 eV and remains highly localized on the same situation (Figure 8).

Chemical hardness reflects a molecule's resistance to intermolecular charge transfer, so a molecule with high chemical hardness or low chemical softness has low chemical reactivity and high kinetic stability [36]. Table 7 demonstrates that the ligand's chemical hardness decreases from 2.99 eV to 2.58 eV upon interaction with the vanadium metal cation, indicating greater chemical reactivity (lower kinetic stability) of the complex relative to the ligand. The electronic chemical potential reflects the tendency of electrons to escape. As shown in Table 7, the ligand has a higher chemical potential than the complex, indicating a high charge transfer from the ligand to the metal cation. The electrophilicity index measures the favorable energy change when a chemical system is saturated with electrons [37]. The calculated ω values indicate that the complex has an electrophilic character, whereas the ligand is nucleophilic. Electron-donating and electron-accepting powers are the desire of a molecule to donate and accept an electronic charge, respectively [38]. Based on the results, the calculated ω^- and ω^+ studied ligand and complex. The complex is noted to have higher values than the ligand.

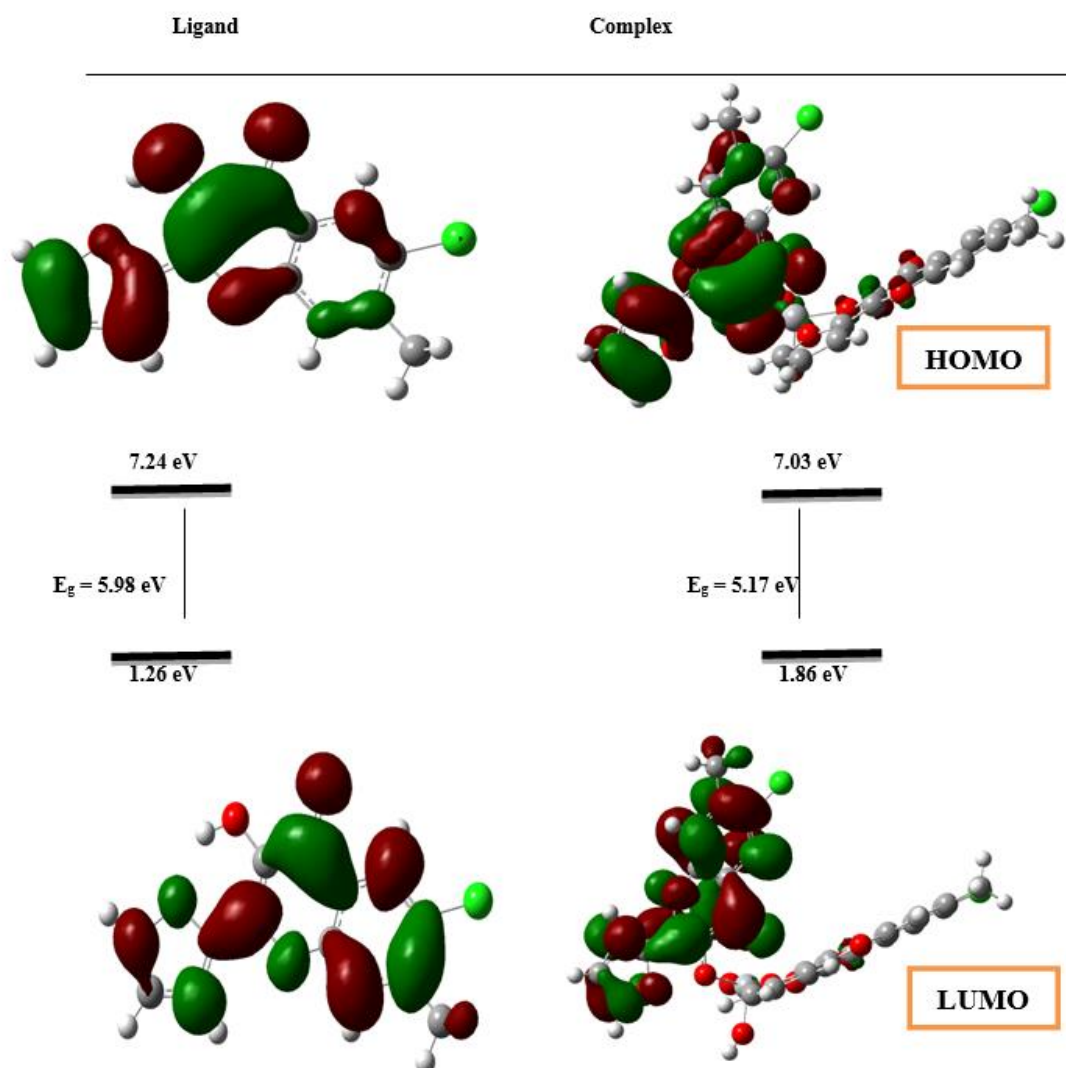


Figure 8. HOMO and LUMO profiles for the studied ligand and complex.

3.5. QTAIM analysis.

In this section, the values of electron density (ρ_{BCP}) and its Laplacian ($\nabla^2 \rho_{BCP}$) as well as total energy density (H_{BCP}), kinetic energy density (G_{BCP}), and potential energy density (V_{BCP}) of the interatomic contacts between the ligand and metal cation for the investigated complex have been calculated, and the obtained results are reported in Table 8. Furthermore, the molecular graph of the complex is depicted in Figure 9, which demonstrates the positions of critical points and their corresponding bond paths between the ligand and metal cation.

The value of ρ_{BCP} is a measure of chemical bond strength, with small and large values corresponding to weak and strong interactions, respectively [39]. As shown in Table 8, the ρ_{BCP} value at the BCP of the V39-O19 bond is higher than that of the other bonds, indicating a stronger interaction between the O19 atom of the Ligand and the V39 metal. The positive values of the $\nabla^2 \rho_{BCP}$ demonstrate a decrease in the ρ_{BCP} values of the interactions, which are called closed-shell interactions, whereas the negative values show shared interactions[40]. Table 8 represents that $\nabla^2 \rho_{BCP}$ values for all the selected bonds are found to be positive, hence indicating the closed-shell interactions.

The negative values of the $\nabla^2 \rho_{BCP}$ and H_{BCP} illustrate strong interactions, whereas the positive value of $\nabla^2 \rho_{BCP}$ and the negative value of H_{BCP} indicates medium interactions. In the case of weak interactions, $\nabla^2 \rho_{BCP}$ and H_{BCP} values are positive [41]. The obtained results demonstrate that the interaction of V39 with the O19, O38, O40, and O41 atoms of the ligand is a medium interaction, whereas weak interactions predominate for the other bonds (V39-O18, V39-O33, and O19-H55).

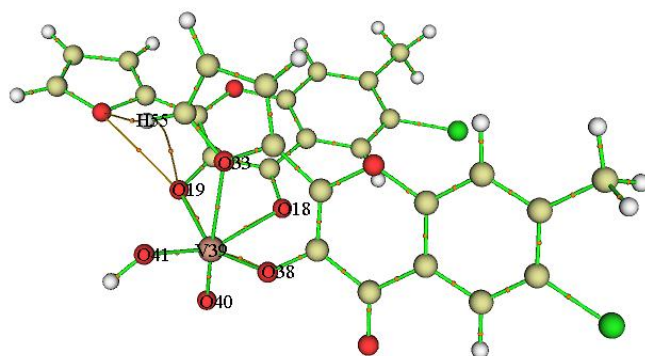


Figure 9. Molecular graph of the studied metal-ligand complex.

Table 8. Calculated topological parameters (a.u) at BCP of the selected bonds.

Bond	ρ_{BCP}	$\nabla^2 \rho_{BCP}$	H_{BCP}	G_{BCP}	V_{BCP}	$-G_{BCP}/V_{BCP}$
V39-O18	0.0600	0.303	0.447	0.713	-0.669	1.065
V39-O19	0.0697	0.470	-0.644	0.124	-0.130	0.953
V39-O33	0.0309	0.152	0.320	0.348	-0.316	1.101
V39-O38	0.0336	0.172	-0.286	0.196	-0.225	0.871
V39-O40	0.0610	0.330	-0.268	0.476	-0.744	0.639
V39-O41	0.0362	0.203	-0.538	0.229	-0.283	0.809
O19-H55	0.0123	0.122	0.175	0.154	-0.112	1.375

To characterize the nature of the interactions, the negative ratio of the kinetic electron energy density to the potential electron energy density ($-G_{BCP}/V_{BCP}$) values is calculated. The ratios of $0.5 < -G_{BCP}/V_{BCP} < 1$, $1 < -G_{BCP}/V_{BCP} < 0.5$, and $-G(r)/V(r) > 1$ indicate covalent, electrostatic, with partially covalent and non-covalent interactions, respectively [42]. As shown in Table 8, the calculated $-G_{BCP}/V_{BCP}$ values for the V39-O19, V39-O38, V39-O40, and V39-

O41 bonds are between 0.5 and 1, indicating that the interactions are mainly electrostatic, with a partially covalent nature. In contrast, this ratio for other bonds (V39-O18, V39-O33, and O19-H55) is greater than unity, meaning they have a non-covalent character.

4. Conclusions

For trace spectrophotometric detection and determination of vanadium in +5 oxidation state, a new binary liquid-liquid extraction approach using 6-chloro-3-hydroxy-7-methyl-2-(2'-furyl)-4*H*-chromen-4-one (CHMFC) as a complexing agent has been developed. The best-suited conditions for forming a 1:2 (M:L) V(V)-CHMFC complex were studied. The resultant complex is yellow and can be used to quantify vanadium at the microlevel in a simple, cost-effective manner. The studied method is a rapid, sensitive ($6.011 \times 10^4 \text{ l mol}^{-1} \text{ cm}^{-1}$) and selective procedure. Good linearity ($r = 0.9987$) is seen up to $1.1 \mu\text{g}$ of V (V) ml^{-1} . The method is very reproducible with adequate precision and accuracy (RSD = 0.298 %), compares favorably to numerous existing methods of vanadium determination [7-14], and is satisfactorily expanded to examine vanadium in a wide range of samples (synthetic and technical). The analytical research is successfully extended to DFT [43-48] calculations to predict the structural shape and establish the complex's ultimate stoichiometry. Quantum theory of atoms in a molecule, the QTAIM [49-51] analysis, well explored and explained the quantum chemical topological features of the electron density and its Laplacian, along with total energy density, kinetic energy density, and potential energy density of the interatomic contacts between the ligand and the metal cation complex under study.

Author Contributions

Conceptualization, N.A. and S.N.; methodology, N.K., C.D. and M.M.; software, R.K. and S.K.; formal analysis, N.A. and S.N.; investigation, N.A. and R.K.; resources, N.A., N.K., C.D. and M.M.; data curation, N.A.; writing—original draft preparation, N.K., M.M. and R.K.; writing—review and editing, N.A.; visualization, N.A.; supervision, N.A. All authors have read and agreed to the published version of the manuscript.

Institutional Review Board Statement

Not applicable.

Informed Consent Statement

Not applicable.

Data Availability Statement

Data supporting the findings of this study are available upon reasonable request from the corresponding author.

Funding

This research received no external funding.

Acknowledgments

The authors express their gratitude to the authorities, Maharishi Markandeshwar (Deemed to be University), Mullana, for providing the required resources for this study.

Conflicts of Interest

The authors declare no conflict of interest.

References

1. Roscoe, H. E.; Researches on vanadium. *Proceedings of the Royal Society of London*. **1869**, *18* (114–122): 37–42. <https://doi.org/10.1098%2Frsp.1869.0012>.
2. Marshall, J. L.; Marshall, V. R. Rediscovery of the Elements: The "Undiscovery" of Vanadium *unt.edu. The Hexagon*. **2004**, p. 45.
3. Moskalyk R.R.; Alfantazi A.M. Processing of vanadium: A review. *Miner. Engg.* **2003**, *16*(9), 793-805. [https://doi.org/10.1016/S0892-6875\(03\)00213-9](https://doi.org/10.1016/S0892-6875(03)00213-9).
4. Chatterjee, M.; Das, S.; Chatterjee, M.; Roy, K. Vanadium in biological systems. *Encycl Metallopro* **2013**, 2293-2297. https://doi.org/10.1007/978-1-4614-1533-6_134.
5. Treviño S.; Díaz A.; Sánchez-Lara E.; Sanchez-Gaytan B.L.; Perez-Aguilar J.M.; González-Vergara E. Vanadium in biological action: chemical, pharmacological aspects, and metabolic implications in diabetes mellitus. *Biol Trace Elem Res*. **2019**.*188*(1), 68-98. doi: 10.1007/s12011-018-1540-6.
6. Rehder D. The role of vanadium in biology. *Metallomics*. **2015**, *7*, 730-742. <https://doi.org/10.1039/C4MT00304G>.
7. Khazal, H. M.; Hussain J.; Khazal, F. Spectrophotometric determination of trace amount of vanadium in rice and flour using 1-[(4-antipyl azo)] 2-Naphthol as new chromogenic spectrophotometry. *J Phys: Conference Series* **2020**, *1660*, 012024, <https://doi.org/10.1088/1742-6596/1660/1/012024>.
8. Saravanska, A.D.; Racheva, P.V.; Divarova, V.V. Extraction-Spectrophotometric and Theoretical Studies on a Ternary Complex Obtained from Vanadium(V) and 4-Nitrocatechol. *Russ J Inorg Chem* **2021**, *66*,1880–1886, <https://doi.org/10.1134/S0036023621120147>.
9. Singh, S.; Agnihotri, N.; Rathi, P.; Agnihotri, R.; Kumar, V. Molecular Dynamics, Biological Study and extractive spectrophotometric determination of vanadium (V)-2-methyl-8-quinolinol complex. *Iran J Chem Chem Eng* **2021**, *40*, 207-214, <https://doi.org/10.30492/IJCCE.2020.93050.3273>.
10. Rajeev, V.; Rajput, S.K. Spectrophotometric Determination of Vanadium (V) using 2-Furohydroxamic Acid as A New Analytical Reagent. *SSRG Inter J Appl Chem* **2021**, *8*, 10-12, <https://doi.org/10.14445/23939133/IJAC-V8I1P103>.
11. Okenwa C.J.; Ukoha P.O.; Chinyere E.C. Quantification and speciation of trac. E amount of vanadium (III) and vanadium (V) using 2-[(e)-[3-[(e)-(2-hydroxyphenyl) methyleneamino] phenyl] iminomethyl] phenol. *J Anal Pharm Res*. **2021**, *10*, 136-145, <https://doi.org/10.15406/japlr.2021.10.00377>.
12. Nikolina, M.; Fatma, G.; Petya, R.; Vassil, D.; Vasil, A.; Kiril, G. An environmentally friendly cloud point extraction–spectrophotometric determination of trace vanadium using a novel reagent. **2021**, *334*, 116086, <http://dx.doi.org/10.1016/j.molliq.2021.116086>
13. Abrarin, S.; Ahmed, M. A highly sensitive and selective spectrophotometric method for the determination of vanadium at nanotrace levels in some environmental, biological, soil, food, and pharmaceutical samples using salicylaldehyde-benzoylhydrazone. *European J Chem* **2020**, *11*, 385-395, <http://dx.doi.org/10.5155/eurjchem.11.4.385-395.2030>.
14. Valdinei, S.; Leonardo, S. G.T.; Joaly, Sthefane, S. O. L.; Uillian M. F. C.; Olívia, M. C. O.; Antonio, F. Q.; Marcos, A. B. Analytical strategies for spectrometric determination of vanadium in samples of interest in the petroleum industry. *Appl Spectrosc Rev* **2020**, *55*, 128-157, <https://doi.org/10.1080/05704928.2018.1542600>.
15. Dong L.H.; Wei W.; Yu C.L.; Hou Z.H.; Zeng Z.; Chen T.; Huang F. Determination of Vanadium Isotope Compositions in Carbonates Using an Fe Coprecipitation Method and MC-ICP-MS. *Anal Chem* **2021**, *93*, 7172-7179, <https://doi.org/10.1021/acs.analchem.0c04800>.

16. Gab-Allah, M.A.; Shehata, A.B. Determination of iron, nickel, and vanadium in crude oil by inductively coupled plasma optical emission spectrometry following microwave-assisted wet digestion. *Chem Pap* **2021**, *75*, 4239–4248, <https://doi.org/10.1007/s11696-021-01633-8>.
17. Amorim, F.A.C.; Welz, B.; Costa, A. C.S.; Lepri, F. G.; Vale, M. G. R.; Ferreira, S. L.C. Determination of vanadium in petroleum and petroleum products using atomic spectrometric techniques. *Talanta* **2007**, *72*, 349–359, <https://doi.org/10.1016/j.talanta.2006.12.015>.
18. Ali, J.; Tuzen, M.; Kazi, T. G. Green and innovative technique develop for the determination of vanadium in different types of water and food samples by eutectic solvent extraction method. *Food Chem* **2020**, *306*, 125638, <https://doi.org/10.1016/j.foodchem.2019.125638>.
19. Filik, H.; Aksu, D. Determination of Vanadium in Food Samples by Cloud Point Extraction and Graphite Furnace Atomic Absorption Spectroscopy. *Food Anal Methods* **2012**, *5*, 359–365, <https://doi.org/10.1007/s12161-011-9254-9>.
20. Rama, M.J. R.; Medina, A. R.; Díaz, A. M. A flow-injection renewable surface sensor for the fluorimetric determination of vanadium(V) with Alizarin Red S. *Talanta* **2005**, *66*, 1333–1339, <https://doi.org/10.1016/j.talanta.2005.01.053>.
21. Berton, P.; Martinis, E. M.; Wuilloud, R. G.; Development of an on-line temperature-assisted ionic liquid dispersive microextraction system for sensitive determination of vanadium in environmental and biological samples. *J Haz Mat* **2010**, *176*, 721–728, <https://doi.org/10.1016/j.jhazmat.2009.11.094>.
22. Mazurova, I.; Khvashevskaya, A.; Guseva, N.; The choice of conditions for the determination of vanadium, chromium and arsenic concentration in waters by ICP-MS using collision mode. *Proc Chem* **2015**, *15*, 201–205, <https://doi.org/10.1016/j.proche.2015.10.032>.
23. Charlot, G.; Bezier, D.; 1957 Quantitative Inorganic Analysis, p 625, Methuen and Co. Ltd., London, URL: https://books.google.co.in/books/about/Quantitative_Inorganic_Analysis.html?id=qyxRAAAAMAAJ&redir_esc=y
24. Algar, J.; Flynn, J.P.; A new method for the synthesis of flavones. *Proc Royal Irish Acad* **1934**, *42B* 1–8, <https://www.jstor.org/stable/20517064>. Oyamada, T.; A new general method for the synthesis of flavonol derivatives. *J Chem Soc Jpn* **1934**, *55*, 1256–1261, <https://www.journal.csj.jp/doi/pdf/10.1246/bcsj.10.182>
25. Frisch, M. J.; et al , Gaussian 03, (Revision B.04), Gaussian, Inc., Wallingford CT, **2004**, <https://gaussian.com/g03citation/>.
26. Frisch, A.; Nielson, A. B.; Holder, A. J.; GAUSSVIEW User Manual .Gaussian Inc. Pittsburgh.PA, **2000**, http://users.df.uba.ar/rboc/em3/GAUSSIAN_TRAIN.pdf.
27. Becke, A. D.; Density-functional thermochemistry III The role of exact exchange. *J Chem Phys* **1993**, *98*, 5648–5652. <https://doi.org/10.1063/1.464913> ; Lee, C.; Yang, W.; Parr, R.G. ; Development of the Colle-solvett correlation energy formula into a functional of the electron density. *Phys Rev B* **1988**, *37*, 785–789, <https://doi.org/10.1103/PhysRevB.37.785>
28. Patersson, G. A.; Al-Laham, M. A. A complete basis set model chemistry.II. Open shell systems and the total energies of the first row atoms. *J Chem Phys* **1991**, *94*, 6081–6090, <https://doi.org/10.1063/1.460447>.
29. Hay, P. J.; Wadt, W. R.; Ab initio effective core potential for molecular calculations. Potentials for the transition metal atoms Sc to Hg. *J Chem Phys* **1985**, *82*, 270–284, <https://doi.org/10.1063/1.448799>
30. Wadt, W. R.; Hay, P. J. ; *Ab-initio* effective core potential for molecular calculations. Potentials for the main group elements Na to Bi. *J. Chem Phys* **1985**, *82*, 284–299. <https://doi.org/10.1063/1.448800>
31. Ringbom, A. On the accuracy of colorimetric analytical methods. I. Fresenius *Z. Anal Chem* **1938**, *115*, 332–343. <https://doi.org/10.1007/BF01753937>.
32. Job, P. Formation and stability of inorganic complexes in solution. *Ann Chim* **1928**, *9*, 113, [https://www.scirp.org/\(S\(351jmbntvnsjt1aadkozje\)\)/reference/referencespapers.aspx?referenceid=1653827](https://www.scirp.org/(S(351jmbntvnsjt1aadkozje))/reference/referencespapers.aspx?referenceid=1653827).
33. Vosburgh, W. C.; Cooper, G. R. The identification of complex ion in solution by spectrophotometric measurements. *J Am Chem Soc* **1941**, *63*, 437, <https://doi.org/10.1021/ja01847a025>.
34. Yoe, J. H.; Jones, A. L. Colorimetric determination of iron with disodium-1,2-dihydroxybenzene-3,5-disulfonate. *Ind Eng Chem (Anal Ed)* **1944**, *16*, 111, <https://pubs.acs.org/doi/10.1021/i560126a015>.
35. Fukui, K.; Yonezawa, T.; Shingu, H. J. A molecular orbital theory of reactivity in aromatic hydrocarbons. *Chem Phys* **1952**, *20*, 722, <https://doi.org/10.1063/1.1700523>.
36. Pearson, R. G.; Palke, W. E. Support for a principle of maximum hardness. *J Phys Chem* **1992**, *96*, 3283–3285, <https://doi.org/10.1021/j100187a020>.
37. Parr, R. G.; Szentpály, L. V.; Liu, S. Electrophilicity index. *J Am Chem Soc* **1999**, *121*, 1922–1924, <https://doi.org/10.1021/ja983494x>.

38. Gázquez, J. L.; Cedillo, A.; Vela, A. Electrodonating and Electroaccepting Powers. *J Phys Chem A* **2007**, *111*, 1966–1970, <https://doi.org/10.1021/jp065459f>.
39. Milenković, D.; Avdovic, E.; Dimic, D.; Sudha, S.; Ramarajan, D.; Milanović, Z.; Trifunović, S.; Marković, Z. S. Vibrational and Hirshfeld surface analyses, quantum chemical calculations, and molecular docking studies of coumarin derivative 3-(1-m-toluidinoethylidene)-chromane-2,4-dione and its corresponding palladium(II) complex. *J Mol Struct* **2020**, *12*, 7935, <https://doi.org/10.1016/j.molstruc.2020.127935>.
40. Rojas-Valencia, N.; Gómez, S.; Guerra, D.; Restrepo, A. A detailed look at the bonding interactions in the microsolvation of monoatomic cations. *Phys Chem Chem Phys* **2020**, *22*, 13049-13061, <https://pubs.rsc.org/en/content/articlelanding/2020/cp/d0cp00428f>.
41. Sanchez-Coronilla, A.; Sanchez-Marquez, J.; Zorrilla, D.; Martin, E.I.; de los Santos, D.M.; Navas, J.; Fernandez-Lorenzo, C.; Alcantara, R.; Martin-Calleja, J. Convergent study of Ru–ligand interactions through QTAIM, ELF, NBO molecular descriptors and TDDFT analysis of organometallic dyes. *Mol Phys* **2014**, *112*, 2063-2077, <https://doi.org/10.1080/00268976.2014.884729>.
42. Khavani, M.; Izadyar, M.; Housaindokht, M. R. DFT investigation and molecular dynamic simulation on the selective complexation of cis-cyclic nanopeptides with alkaline earth metal ions. *Sens Actuators B Chem* **2015**, *221*, 1120-1129, <https://doi.org/10.1016/j.snb.2015.07.090>.
43. Mohmad, M.; Agnihotri, N.; Kumar, V.; Kumar, R.; Kaviani, S. Iridium (III)-3-hydroxy-2-(3'-methyl-2'-thienyl)-4-oxo-4H-1-benzopyran Complex: The Analytical, In-vitro Antibacterial and DFT Studies. *Inorg Chem Comm* **2022**, *139* 109333, <https://doi.org/10.1016/j.inoche.2022.109333>.
44. Dhonchak, C.; Agnihotri, N.; Kumar, A. Zirconium (IV)-3-hydroxy-2-tolyl-4H-chromen-4-one complex- the analytical and DFT studies. *J Mol Model* **2021**, *27*, 336, <https://doi.org/10.1007/s00894-021-04949-0>.
45. Mohmad, M.; Agnihotri, N.; Kumar, V.; Azam, M.; Al-Resayes, S. I.; Kamal, R.; Kumar, R.; Alam, M.; Kaviani, S. Radical Scavenging capacity, Antibacterial Activity, and Quantum Chemical Aspects of the Spectrophotometrically Investigated Iridium (III) complex with benzopyran derivative. *Front Pharmac* **2022**, *13*, 945323, <https://doi.org/10.3389/fphar.2022.945323>.
46. Dhonchak, C.; Agnihotri, N.; Javed, S.; Khanum, G. Spectroscopic Quantum Chemical and Molecular Docking Study of 5,7-Dibromo-8-Quinololinol and Its Spectrophotometrically Investigated Niobium (V) Complex. *Polycycl Aromat Compd* **2022**, <https://doi.org/10.1080/10406638.2022.2097280>.
47. Mahmoud, N.H.; Elsayed, G. H.; Aboelnaga, A.; Fahim, A. M. Spectroscopic studies, DFT calculations, cytotoxicity activity, and docking stimulation of novel metal complexes of Schiff base ligand of isonicotinohydrazide derivative. *App Organomet Chem* **2022**, *36*, <https://doi.org/10.1002/aoc.6697>.
48. Aggoun, D.; Messasma, Z.; Bouzerafa, B.; Berenguer, R.; Morallon, E.; Ouennoughi, Y.; Ourari, A. Synthesis, characterization and DFT investigation of new metal complexes of Ni (II), Mn (II) and VO (IV) containing N, O-donor Schiff base ligand. *J Mol Str* **2021**, *1231*, 129923, <https://doi.org/10.1016/j.molstruc.2021.129923>.
49. Lepetit, C.; Kahn, M.L. QTAIM and ELF topological analyses of zinc-amido complexes. *Res Chem Intermed* **2021**, *47*, 377–395, <https://doi.org/10.1007/s11164-020-04328-z>.
50. Dhonchak, C.; Agnihotri, N.; Mohmad, M.; Thakur, A.; Kumar, A.; DFT Studies of Zr(IV) - 3-Hydroxy-2-[2'-(5'-methylthienyl)]-4H-chromen-4-one Complex. *Res J Chem Environ* **2022**, *26*, 137-141, <https://doi.org/10.25303/2606rjce137141>
51. Kowsalya, P.; Neelakantan, M. A.; Bhuvanesh, Nattamai S. P.; Tetranuclear Cu(II) complex with [2+4] Cu₄O₄ cubane based core framework derived from 2-[(2-(1-hydroxy-ethyl)-phenylimino)-methyl]-6-methoxy-phenol: Quantifying conventional and unconventional interactions and QTAIM analysis. *J Mol St* **2022**, *1254*, 132396, <https://doi.org/10.1016/j.molstruc.2022.132396>.